1992 Space Science Reviews, Reprinted, with permission, from Space Science Reviews, Vol. 60, 1992.

GALILEO PHOTOPOLARIMETER/RADIOMETER EXPERIMENT

E. E. RUSSELL. F. G. BROWN, R. A. CHANDOS, W. C. FINCHER.L. F. KUBEL

Santa Barbara Research Center. Goleta, CA 93017, U.S.A.

A. A. LACIS and L. D. TRAVIS

Goddard Space Flight Center, Institute for Space Studies, New York, NY 10025, U.S.A.

Abstract. The Photopolarimeter/Radiometer (PPR) is a remote sensing instrument on the Galileo Orbiter designed to measure the degree of linear polarization and the intensity of reflected sunlight in ten spectral channels between 410 and 945 nm to determine the physical properties of Jovian clouds and aerosols, and to characterize the texture and microstructure of satellite surfaces. The PPR also measures thermal radiation in five spectral bands between 15 and 100 μm to sense the upper tropospheric temperature structure. Two additional channels which measure spectrally integrated solar and solar plus thermal radiation are used to determine the planetary radiation budget components. The PPR photopolarimetric measurements utilize previously flown technology for high-precision polarimetry using a calcite Wollaston prism and two silicon photodiodes to enable simultaneous detection of the two orthogonal polarization components. The PPR radiometry measurements are made with a lithium tantalate pyroelectric detector utilizing a unique arrangement of radiometric stops and a scene/space chopper blade to enable a warm instrument to sense accurately the much colder scene temperatures.

1. Introduction

The Galileo Photopolarimeter/Radiometer (PPR) is designed to measure the degree of linear polarization (and intensity) of reflected sunlight and the intensity of the thermally emitted infrared radiation from Jupiter and its major satellites. The PPR combines the high-precision polarimetry capability of predecessor instruments flown on the Pioneer 10 and 11 and Pioneer Venus missions with the capability of obtaining thermal infrared measurements for temperature sounding and radiation budget studies.

Many of the basic optical, mechanical and electronic design features of the PPR are based upon proven techniques employed on precursor instruments designed and fabricated at the Santa Barbara Research Center. The Imaging Photopolarimeter (IPP) instrument (Pellicori *et al.,* 1973) was flown on both the Pioneer 10 and 11 spacecraft, successfully obtaining imaging, polarimetry and photometry of Jupiter and Saturn (flybys) and interplanetary observations of zodiacal light. These instruments are still functioning and are being used by mission control for spacecraft navigation purposes now that they have left the solar system. Using some of the features of the IPP, the Cloud Photopolarimeter (CPP) instrument (Watts *et al.,* 1977) was designed and built for the Pioneer Venus Orbiter spacecraft launched in 1978. With more than 12 years of flawless operation, the CPP continues to provide images and polarimetry maps of the Venus clouds, yielding the most extensive climatology for any planet other than the Earth.

Following a brief description of the scientific objectives of the PPR experiment, we describe the optical and electronic hardware of the instrument, its basic functions and calibration. Finally, we present a brief summary of the expected instrument signal to noise ratio (SNR) performance characteristics.

2. Scientific Objectives

The primary science objectives and anticipated results of the PPR experiment are to: (1) determine the vertical and horizontal distribution of cloud and haze particles in the atmosphere of Jupiter, including their size, shape and refractive index; (2) determine the energy budget of Jupiter and the variation in amount and spatial distribution of reflected solar radiation and emitted thermal radiation for Jupiter and its satellites, including the thermal structure of the atmosphere and the vertical distribution of absorbed solar radiation in the atmosphere of Jupiter, and (3) measure and map the photometric, polarimetric, and radiometric properties of the major satellites of Jupiter.

The polarimetric and photometric measurements made by the PPR will permit determination of the vertical cloud structure of Jupiter, including also the cloud particle size, shape, and refractive index. The spectral bands used for this purpose are illustrated in Figure 1 and their spectral characteristics are summarized in Table I. Basically, the polarimetric channels are situated in continuum regions at 410, 678.5, and 944.6 nm spaced as widely as possible to provide the broadest spectral baseline commensurate with SNR greater than 2000. The measurements yield the precision polarimetry necessary to separate cloud micro-structure information from Rayleigh scattering and thus enable deduction of cloud-top heights and cloud vertical distribution.

The photometric channels shown in Figure I also yield polarimetric information of comparable precision, provided the polarization direction is known. This follows because the photometric channels utilize the same detectors and optical elements used for polarimetry, except for the absence of repeated retarder position measurements used for polarimetry. The photometric channels at 633.3 and 829.3 nm provide additional spectral constraints in the continuum regions of the spectrum, advantageous in separating cloud, haze, and 'chromophore' contributions. The photometric channels at 618.7, 840.3, and 891.8 nm are located within medium, weak, and strong CH4 bands, respectively, and will be instrumental in further constraining the cloud vertical structure. The 648.0 and 788.7 nm channels measure weak and medium NH3 absorption, respectively, and will permit mapping of the NH3 distribution at visible wavelengths.

A primary objective of the PPR radiometric measurements is to determine the radiative energy balance of Jupiter. This will be accomplished by differencing measurements obtained in the Solar + Thermal channel (0.3-110,mm) and measurements in the Solar Only channel (0.3-4, mm). Voyager results (Hanel *et al.,* 1981) indicate that the emitted thermal radiation from Jupiter tends to be globally uniform and exceeds the latitudinally dependent absorbed solar radiation by a factor of 1.7 (globally averaged). The ratio of emitted-to-absorbed radiation and its latitudinal dependence, fundamental for understanding the internal structure and evolution of Jupiter, will be measured by the PPR with improved accuracy. The expected SNR for these measurements at Jupiter is ~500. With the more complete geometrical coverage available from an orbiting platform, the PPR measurements will significantly improve on our knowledge of the Pioneer-derived planetary phase integral (Tomasko *et al.,* 1978) and thus of the global Jovian radiative energy balance.

The PPR will also make radiometric measurements in five broad-band spectral channels spanning 15 to 110 μm. The placement of these channels relative to the Jovian thermal spectrum is shown in Figure 2, and their spectral bandpasses are given in Table I. These radiometric channels were incorporated into the PPR design to provide a measure of temperature sounding in the 60 to 600 mb region of the atmosphere. These measurements will help to relate the observed cloud and thermal structure with the atmospheric dynamics of Jupiter. Channels *A*, *B*, and *C* in Figure 2 will also measure the spatial variations in ortho-para distribution which is an important tracer of deep atmospheric circulation. Channels *D* and *E* will sample radiation from deeper atmospheric regions with channel *D* having some sensitivity to the ammonia cloud layer, while channel *E* will, in addition, have sensitivity to the vertical NH3 distribution. The SNR performance of the temperature sounding spectral channels, however, is less than optimum (see Table VI), and will require measurement strategies to permit data averaging in order to build up the SNR.

The full complement of PPR photometric, polarimetric, and radiometric measurements will also be applied to the Jovian satellites and to other targets of opportunity. The photometric and polarimetric measurements over a wide range of phase angles will yield information on the nature of satellite surface material in regard to texture and composition. The radiometric measurements, taken under different conditions of solar illumination, will provide additional information on the texture and heat capacity of the satellite surface material. For typical satellite encounter altitudes of 1000 km, the spatial resolution of PPR measurements will be 2.5 km, comparable to much of the better Voyager imaging resolution.

The photometric, polarimetric, and radiometric measurements obtained by the PPR will provide phase angle and zenith angle coverage of Jupiter and of its satellites that is not possible for ground-based observations. These measurements will provide important new information that will permit more definitive determinations of the vertical cloud structure and of the cloud and haze micro-structure in the cloud-top region. They will also improve our knowledge of the global Jovian energy balance and will help characterize possible time and/or spatial variations in the solar and thermal components of the radiation budget of Jupiter.

3. Instrument Description

The PPR is a multi-purpose and multi-function instrument designed for both solar wavelength photopolarimetric and thermal infrared measurements. The PPR is a 5.2 kg instrument with a 10 cm Cassegrainian Dall-Kirkham telescope. The overall dimensions of the PPR are 45 x 19 x 33 cm. A pictorial view of the PPR is shown in Figure 3.

Figure 4 is an exploded view of the PPR illustrating the main functional elements of the instrument. The main housing of the PPR mounts onto the top of the electronics, which consists of a set of four stacked modules which, in turn, are mounted onto the baseplate. The main housing supports the scene-view and space-view telescopes along with the ancillary optical elements, the filter/retarder motor, the chopper, and the detectors and associated pre-amplifiers. The key optical elements of the PPR contained within the main housing are shown pictorially in Figure 5.

For polarimetry and photometry measurements, the flux from the scene is collected by the scene-view telescope and focused onto a circular field stop subtending 2.5 mrad. Flux passed by the field stop then is modified by passage through optical elements located on the filter/retarder wheel. At the polarimetry positions, the flux passes through a halfwave retarder and a spectral filter, while at photometry positions it passes only through a filter. The relay lens directs the flux through the Wollaston prism which serves as a polarizing beam-splitter and produces two spatially-separated and orthogonally-polarized output beams. The detector lenses focus these beams onto the two silicon photodiodes. For polarimetry and photometry measurements the chopper is stationary and is positioned so as not to block the scene flux.

During radiometry measurements, the chopper is operated at 30 Hz and alternately directs the flux from the scene-view and space-view telescopes through the field stop. At each radiometry position the flux passed by a radiometry filter is reflected radially outward from the filter/retarder wheel by means of an ellipsoidal mirror (one mounted on the wheel at each of the seven radiometry positions). The flux reflected by the ellipsoidal mirror is collected by a condensor system consisting of a truncated conical reflector with a small diamond lens mounted onto the small end of the cone. The focused, modulated flux is detected by a lithium tantalate pyroelectric detector. The alternative views from the scene-view and space-view telescopes allow the scene radiance to be referenced to the space background (approximately to a 3K blackbody). Also indicated in Figure 5 are four optical elements designated as 'radiometric stops' which serve to restrict the modulated flux reaching the detector to that received from the scene or space, or from the internal instrument elements which are radiometrically 'balanced' to first order. These radiometric stops together with careful preflight calibration, temperature monitoring of key optical elements, and an accurately-monitored, high emittance inflight calibration target (the RCT-PPR), are key to performing radiometrically useful measurements on a 'cool' scene, such as Jupiter, with the 'warm' PPR instrument.

The primary characteristics and instrument description of the PPR are summarized in Table II. The upper portion of the table lists the general instrument properties, while the lower portion indicates features associated with the

three primary measurement functions provided by the PPR.

3.1. OPTICAL DESIGN

3.1.1. *Telescopes*

The 10-cm aperture scene-view telescope is a Cassegrainian Dall-Kirkham design which gives excellent image quality for the 2.5 mrad (0.14°) instantaneous field of view, with the image quality being dominated by diffraction at the longer wavelengths. The view of space in radiometry mode is via reflection from the chopper mirror and the planar space-view telescope mirror. The telescope assemblies, including the mirrors themselves, are fabricated of beryllium which thermally match the beryllium main housing and together yield significant mass savings. The mirrored surfaces are nickelplated and overcoated with aluminum. This choice of mirror finish yields a highly durable mirror with good spectral performance over the extended spectral range of interest.

3.1.2. *Radiometric Stops*

As indicated in Figure 5, two radiometric stops are used on the scene-view telescope assembly, one is mounted adjacent to the secondary mirror (between the primary and secondary mirrors) and the other on the back of the primary mirror (between the primary mirror and the field stop). These are designated as RS 1A and RS 1B, respectively, with the identifier '1' denoting use in the scene-view beam and the modifier 'A' or 'B' indicating the relative positioning along the optical axis. The optical surfaces of these radiometric stops are spherical with the radius of curvature of each being equal to the distance of the radiometric stop from the field stop (the aperture defining the instantaneous field of view). As viewed from the field stop, RS 1A is configured to block the view of the secondary mirror obscuration, to block the three secondary mirror support arms, and to define the viewed outer perimeter of the primary mirror. In a similar manner, RS1B spans an annular solid angle which blocks the outer perimeter of RSlA and extends to beyond the angular response of the radiometry channel (pyroelectric detector plus lens/cone/relay mirror). This is shown schematically in Figure 6. The spherical surfaces of the radiometric stops are gold coated to provide a high reflectance (low emittance) in the spectral region where thermal emission of the instrument is significant.

During the installation of RS 1A and RS 1B, both elements are tilted slightly such that an area approximately 3 mm from the field stop is imaged by the two radiometric stops through the field stop. This area imaged has a machined, pyramidal array-shaped structure to increase the effective emittance of this reference target to near unity. (A more conventional, conical target could not be used since the depth dimension is limited to approximately 1.5 mm by the proximity of the chopper mirror and filter wheel.) Thus, the detector alternately views the scene radiance plus the radiance from the scene-view mirrors and radiometric stops and the reference target (via imaging by the radiometric stops) and then space radiance plus the near equivalent elements in the space-view optical path.

The rear surface of the chopper mirror is optically polished and coated in the same manner as the front surface. This feature together with a second high emittance target (mounted orthogonal to the plane of the field stop) prevents the detector from viewing ill-defined portions of the instrument during the portion of the chopping cycle when the scene-view is partially blocked, i.e., as the chopper mirror partially covers the field stop. This viewing situation results from the image inversion that occurs during reflection from the radiometric stops. During the transition period (between viewing only the scene or only space) a varying portion of the rear of the chopper mirror is viewed, and with the present design, a varying portion of the second target is viewed via reflections from the rear surface of the chopper and from the radiometric stops. Thus, this arrangement assures that no large transients associated with viewing ill-defined portions of the instrument occur during the chopper mirror transition period.

The space-view telescope assembly has two radiometric stops, RS2A and RS2B, that serve optically identical roles to the two radiometric stops in the scene-view telescope assembly. The radiometric stops RS2B and RS 1 B are identical parts, while stops RS2A and RS 1A are optically identical, but the support structures are different as they mount on entirely different assemblies.

3.1.3. *Filter/Retarder Wheel Optical Elements*

Located on the filter/retarder wheel are spectral filters used to define the required spectral bandpass, the

halfwave retarders used for the polarization analysis of the scene, and the ellipsoidal mirrors used to direct scene flux towards the radiometry detector. The sequential arrangement of the polarimetry, photometry, and radiometry filter positions are illustrated in Figure 7. The filter bandpasses and their spectral locations are summarized in Table I.

The photometry and polarimetry filters are of conventional multilayer design. The materials used for the blocking elements of the filters were prescribed based on the results of radiation testing of candidate optical materials. The difficult spectral requirements for the radiometry filters used designs based on the techniques developed by Seeley *et al.* (1981). A low transmittance problem for the *E* (> 45 μm) filter was solved by combining the long-wavepass multilayer element with a 0.7 mm Z-cut crystal quartz element AR-coated with parylene.

The halfwave retarders were similar in design to those used on the Cloud Photopolarimeter flown on the Pioneer Venus mission. Since the halfwave retarders are located in an f/5 beam, a key feature of the design was a large angular acceptance. This was achieved for the three polarimetry bands by combining crystalline elements of positive and negative birefringence (MgF_2/Al_2O_3 for the 410 nm band and SiO_2/Al_2O_3 for both the 678 and 945 nm bands). The crystalline elements were bonded together with a third element of fused silica to provide the same optical thickness for all three retarders. This configuration of each retarder has sapphire (Al_2O_3) and fused silica as the outer elements with the exposed surface of the sapphire AR-coated to minimize retardance variations due to internal reflections.

The seven small mirrors located on the filter/retarder wheel are off-axis sections of an ellipsoid. These direct scene flux passed by the radiometry filters radially outward toward the radiometry channel detector assembly.

3.1.4. *Aft Optics*
Pupil imaging (refering to the exit pupil of the telescope) is provided in each channel of the PPR in order to obtain uniform photometric response across the field of view. This eliminates the introduction of possible polarimetric errors due to spatial non-uniformity of the detectors and of the scene radiation sensed by the detector. In the case of radiometry, the ellipsoidal filter wheel mirrors together with the cone/lens of the radiometry assembly relays the scene flux onto the 0.57 mm lithium tantalate pyroelectric detector.

3.1.5. *Stray Light Baffles*
The baffle system for the scene-view and space-view telescopes are of conventional ring-baffle design. The ring baffles are sized and located to prevent any ray incident through the entrance aperture that reflects from the side wall of the baffle from reaching the primary mirror with less than one additional reflection. Due to the electrostatic discharge (ESD) requirements imposed on the Galileo instruments, it was necessary to passivate the beryllium baffle with a conductive chemical conversion coating. The baffle interior was painted, since the more usual black anodized finish results in a non-conductive surface. A small amount of carbon was added to the black paint (by ball milling to provide a uniform mix of the carbon), and this provided sufficient electrical conductivity to satisfy the ESD requirements while maintaining the low reflectance of the paint.

As part of the instrument calibration, preliminary measurements were made to characterize the off-axis light rejection of the PPR optical system. A more complete determination of stray light rejection as a function of angle from the PPR optical axis will be performed during inflight calibration opportunities (including also the boresighting of the PPR with respect to other Galileo instruments) by viewing such astronomical objects as stars and spatially unresolved planets.

3.2. MECHANICAL DESIGN

3.2.1. *Mechanical Structure*
Except for the electronic modules, the basic PPR structural elements are beryllium. This choice provides high stiffness with low mass and excellent stabilty. However, additional safety factors as a result of more stringent fracture analysis criteria applicable late in the program removed some of the relative advantages of beryllium versus aluminum. As noted in the Optics Section, the majority of the metal optics components were fabricated

with nickel-plated beryllium. The electronics modules, for which substantial radiation shielding was required, were made of aluminum. Machinable tungsten was used to provide suitable shielding around the more radiation-sensitive elements such as the radiometry channel J-FETs and the analog-to-digital (A/D) converter.

3.2.2. *Mechanisms*

The principal mechanisms of the PPR are the filter/retarder wheel motor, the scene/space chopper, and the scene- and space-view telescope contamination cover actuators. The filter/retarder wheel motor is a 32-position (11.25°/step) direct-drive, stepper motor which is accurately indexed at each wheel position by means of frictionless permanent magnet detenting. Special low magnetic remanence materials and winding techniques maintain tightly coupled flux paths to minimize stray static and dynamic fields. A pin-disk mechanical encoder identical to that used on the Pioneer Venus CPP is used to indicate the filter/retarder position.

The resonant reflective chopper assembly is an electromagnetically driven tuning fork with a mirror and thermistor temperature sensor on one tine and a counterweight on the other tine. The basic design includes special modifications to withstand the launch environment.

Thermal motors, in the form of heated bi-metallic springs, are used to drive the contamination covers of the scene-view and space-view telescopes to their closed position. The actuator springs are wound in the shape of a watch spring with a heater wire attached to one side. The covers normally remain open, but when powered by the PPR replacement heater power, they can be closed during attitude control thruster firings. The mechanism is failsafe in the sense that if a heater were to fail, the cover would remain open. For launch, the covers were secured by latches that were released at the initial inflight checkout by a pair of redundant squibs (bellows actuators).

3.2.3. *Thermal Control*

The PPR is conductively isolated from the scan platform to allow lower temperature operation for improved radiometry channel performance. The instrument is blanketed with multi-layer insulation except for the telescope apertures, the telescope covers, and an exposed area on the side of the main housing. This area (140 cm^2) on the side of the housing is exposed to space to help maintain the PPR operating temperature near -15 °C. The instrument thermal analysis was used to establish the size of this area, with preflight verification being obtained, where possible, during spacecraft system thermal/vacuum testing.

3.3. Electronics

The low power electronics for the PPR instrument retains much of the radiation-proven circuitry from the predecessor instruments built for the Pioneer missions, but most of the discrete control logic has been replaced by a radiation-hard CMOS microprocessor system. The functional block diagram shown in Figure 8 indicates the principal elements of the PPR electronics. The analog circuitry consists of two silicon photodiode polarimetry/photometry channels, one pyroelectric radiometry channel, and an analog multiplexer which presents the three signal channels and the temperature telemetry channels to the 12-bit analog to digital converter. The digital circuitry decodes the serial spacecraft commands and formats the instrument signal and telemetry data for transfer to the spacecraft via the command and data bus. The digital system also provides timing signals for analog channel and mechanism controls. The power subsystem conditions the 30 vdc spacecraft input power and provides the necessary regulated and filtered voltages for instrument operation. This subsystem also contains the power driver circuitry for the actuator controls and calibration lamp.

3.3.1. *Analog Processing*

Pre-amplifiers for all the detector channels are mounted in the optical housing near the detectors. The silicon detectors are operated at zero bias by low-offset transimpedance pre-amplifiers with 100 megohm feedback resistors. Zero bias operation was chosen so that increased detector dark current caused by radiation damage would not saturate the sensitive pre-amplifiers. The slightly increased detector capacitance resulting from zero bias operation does not affect the pre-amplifier noise performance, which is limited by the thermal noise of the feedback resistor.

The pyroelectric detector, the 10^{11} ohm load resistor, and the low-noise junction field effect buffer transistor (J-FET) are mounted in a small custom detector package. The detector element alternately receives scene radiation and space reference radiation as relayed by the reflective 30 Hz optical chopper assembly, which operates only in radiometry filter wheel positions. The waveform is asymmetrical because the rest position of the chopper must be clear of the optical path to allow photopolarimetry operation. In spite of the extremely high impedance load resistor and J-FET circuitry, sample radiation testing has ensured operation at exposures exceeding 10^5 rads. The remaining pre-amplification stages include boost compensation for the electrical and thermal time constant of the detector element making the 30 Hz output waveform amplitude accurately represent the scene/space flux difference.

Variable-gain signal amplification is provided by electronics in the top section of the electronics module with the gains set in discrete steps in response to instrument commands. The polarimetry/photometry channels incorporate sixteen gain steps spaced a factor of 1.4 apart. These are mechanized by junction FETs switching feedback resistors in the three operational amplifier gain stages. Since it is possible for radiation induced offsets in these stages to degrade the data (particularly at high gains), a dc restore loop is included which acts as a sample and hold circuit, forcing the channel offset to zero when the filter wheel blocks the optical path at specified positions between active filter wheel positions.

The radiometry channel incorporates four FET-switched gain steps spaced a factor of 2 apart. DC restoration is not required because the stages are capacitively coupled to pass the 30 Hz signal waveform. Transient suppression clamp diodes are used at both ac coupling capacitors to rapidly settle the quiescent operating point with each filter position change. A gated full wave synchronous demodulator converts the 30 Hz waveform to a scene proportional dc level. Gating the demodulator serves both to eliminate the effects of spurious optical reflections as the chopper enters and leaves the optical path, and to balance the asymmetrical signal waveform. An intentional signal offset of about 30% of full scale is introduced in the demodulator to ensure that the channel will not saturate if the signal phase reverses. This can occur when viewing a low radiance scene if the optical elements in the space-view telescope are warmer than those in the scene-view telescope such that the net instrument thermal signal exceeded the scene signal.

Electrical low pass filtering is provided for all three signal channels by integration using a resetting integrator circuit. Integration times are synchronized to and include an integer number of radiometry chopper cycles. Integration times of 0.233 and 0.467 s are used for the polarimetry/photometry and radiometry channels, respectively. Four FET-switched resistors (controlled by the microprocessor) at each integrator input adjust the integrator gain in order to partially balance the signal levels for the various filter positions. When all four FETs are switched off, the integrator holds the final signal value, eliminating the need for a sample and hold circuit. Another FET switch then zeros the integrator for the next signal sample.

Signal multiplexing for the data channels and temperature telemetry circuits is accomplished by radiation-hard J-FET high level FET switches identical to those used in previous instruments. Higher density MOS devices were considered, but rejected because of the cost of the extensive radiation testing required in this critical signal switching area. Thermistors for telemetering the optical element temperatures are submultiplexed using similar circuitry to that used in the main multiplexer. Each thermistor is unpowered when it is not being telemetered so that self-heating error is entirely eliminated. A ground command option, however, allows the thermistor on the tuning fork chopper to remain powered to slightly raise the temperature of the chopper mirror during one portion of the PPR radiometric calibration (optical element heater testing). Two ground commendable temperature ranges are provided in the thermistor scaling amplifier to ensure high readout resolution throughout the possible inflight temperature range. Platinum resistance thermometers are used to read out the temperature of the radiometric calibration target (RCT-PPR). These require more scaling circuitry to operate than the thermistor channels, but provide an accurate and stable, long-life temperature measurement capability for the RCT-PPR. All multiplexed channels are digitized to 12 bits by a low power CMOS A/D converter.

3.3.2. *Digital Circuitry*

The digital circuitry centers around the RCA 1802 microprocessor hardware which was supplied and radiation tested by the Galileo Project. Because of the low data rate and simplified conceptual design of the instrument,

only 256 bytes of random access memory are required, and the entire instrument operating system is contained in less than 4K bytes of read-only memory. Clock reference for the microprocessor is formed by doubling the spacecraft supplied 866 kHz clock signal, and all instrument operations are synchronous with clock transitions. Bi-directional spacecraft communications of commands and data are performed using a transformer-coupled bus interface unit (also supplied by the Galileo Project). Microprocessor communication to the PPR electronics is accomplished using I/O port controllers. Most port signals are buffered to eliminate possible failure modes which could damage the microprocessor bus and cause total instrument failure.

In spite of the small ROM memory size, the instrument control program is extensive, controlling all of the commendable optional functions, the command processing and data formatting, the instrument analog and multiplexer timing, the closed-loop filter/retarder wheel and chopper operation, and the power system synchronization. A 3-byte PPR configuration control command is used to select the detailed operation of the PPR. Figure 9 illustrates typical PPR operation in the cycle mode as the instrument steps through the polarimetry, radiometry, and photometry measurement sequences, with the dc restore, chopper initiate, chopper stop and cal lamp activate functions indicated. The commendable functions of the PPR and their brief description are summarized in Table III.

3.3.3. *Actuator Controls*
The 32-position filter/retarder wheel is driven by three sets of bipolar transistor switches, which are in turn controlled from 6 bits of a microprocessor port. The binary brush-type encoder located in the filter/retarder motor is read into another port, thereby giving full closed-loop position control to the microprocessor. To ensure rapid motor damping in the final filter position, the processor momentarily turns on the appropriate motor switches to short the motor windings, thus allowing the motor to be stepped in less than 0.2 s. The brush-type encoder and filter motor were unchanged from the previous Pioneer Venus Orbiter CPP- instrument, having demonstrated extreme reliability (more than 12-year operation in Venus orbit).

Amplitude and phase control are provided for the tuning fork chopper by a combination linear and switching servo system. The tine driver coil is energized by pulsewidth-modulated bipolar transistor switches, and the signal from the tine position feedback coil is processed to provide a linear amplitude error signal. Zero crossings of the feedback signal are phase-compared with a chopper reference pulse from the microprocessor. The servo electronics then meter an appropriate width and timed drive pulse to correct both the amplitude and phase error during each chopper cycle. Servo control is complex because of the requirement to rapidly accelerate the chopper when entering the portion of the filter/retarder wheel containing the radiometry positions and then to damp the oscillations to unblock the optical path when starting the photometry filter positions. Rapid acceleration is obtained by applying a higher than normal power turn-on pulse, and active damping is achieved by reversing the phase of the pickoff signal, thereby providing negative feedback until the fork position feedback signal is small enough to ensure that the optical path is clear.

3.3.4. *Power Subsystem*
Power converter circuitry, located in the bottom section of the electronics module, operates from the 30 V balanced dc spacecraft bus. Bus protection is provided by redundant instrument fuses, EMI filters, and in-rush current limiting inductors. There are two separate transformer coupled power converters, one to supply the pulsed power for the actuators and calibration lamp, and the other to supply the 'cleaner' electronics power. A low-headroom, wide-bandwidth series regulator supplies the electronics converter to ensure that spacecraft bus voltage transients are not transferred to the electronics loads. Both converters are synchronized to a sub-multiple of the spacecraft clock signal. The power supply module also contains all of the power transistor switches for the actuator controls as well as the calibration lamp precision voltage regulator so that EMI generated by the current surges is confined inside the power supply. The 28 V motor voltage is used as input to the calibration lamp series regulator so that regulator failure will cause the 5 V lamp to burn out, though otherwise allowing normal instrument operation (but without calibration). A ground commendable relay switches the calibration lamp regulator from the internal lamp to another lamp located within the RCT-PPR mounted on the spacecraft.

Electronics supply voltages are LC-filtered and regulated using monolithic linear regulators operated with low headroom for efficiency. The logic supply is unregulated, relying on the pre-regulated input to the electronics

converter. Nominal instrument power consumption is 3.8 W without actuator operation, increasing to approximately 11 W during the short duration filter/retarder motor steps.

4.1. PREFLIGHT CALIBRATION

The preflight testing of the assembled PPR consisted of tests performed to verify the mechanical integrity and stability of the instrument (environmental tests such as vibration and temperature cycling) and those associated with the characterization of instrument performance and calibration. Consistent with the scope of this paper, only the latter type of testing will be discussed here. (The instrument thermal/vacuum testing often is performed in a manner to satisfy simultaneously the calibration and environmental test functions.) The performance and calibration testing can be broadly divided into those tests done at ambient temperature and pressure in a laboratory environment and those performed in a thermal/vacuum chamber. Some of the more important preflight calibrations are shown in Table IV. Several of these tests which are important to the ultimate performance of the instrument or have novel or less well-known implementations will be described in the following.

4.1.1. *Ambient Calibrations*

Of particular importance here are the optical calibrations. These include the measurement of the radiometric calibration of the channels that measure the radiance resulting from reflection of the incident solar flux. Due to the spectral radiance differences between the sources used in the radiometric calibrations and the scene radiance, relative spectral response measurements were made on the wide PPR spectral bands, namely, the polarimetry band and the solar reflectance band. The relative spectral response for the other PPR bands was determined from individual component measurements. The majority of the detailed polarimetric calibrations also were performed in an ambient environment. Supplemental measurements to assess any air-to-vacuum and temperature-dependent instrument response were performed as a part of the thermal/vacuum environment testing.

4.1.2. *Radiometric Calibration (Photopolarimetry Channels)*

Halogen-cycle tungsten-filament lamps with spectral irradiance calibrations traceable to the National Institute of Standards and Technology (NIST) were used in a fixed geometry with a diffuse reflectance target of known characteristics. The lamp spectral irradiance uncertainty is better than 1.35% (3σ NIST uncertainty value) with an additional estimated transfer uncertainty of 0.7% over the photopolarimetry spectral range. The reflectance target consists of pressed Halon (polyfluoroethylene) fabricated by a well-controlled procedure to produce a target of known bi-directional reflectance (Weidner and Hsia, 1981). The target is illuminated at normal incidence at a fixed source-to-target distance (100 cm) and is viewed at a 20° angle of incidence. During each of these PPR radiometric calibrations (spanning a period of more than 6 years between the first and last 'final calibration'), measurements were taken with two different lamps to permit cross-checking between the resultant calibrations and to improve the likelihood that during any future calibration the same lamp would be available. The above considerations provide the basis for estimating the PPR radiometric calibration accuracy.

4.1.3. *Radiometric Calibration (Thermal Channels)*

The preflight radiometric calibration of the thermal channels was performed as part of the thermal/vacuum environmental testing of the instrument. For this purpose, blackbody targets were designed to overfill the apertures of the scene-view and space-view telescopes. These blackbody calibrator units, designated BCU- 1 and BCU-2, are identical except that the aperture diameter of BCU-1 is larger than for BCU-2 in order to accommodate the larger scene-view telescope. The BCUs are conical blackbody sources with a 30° apex angle. The interior conical surfaces are painted with a gloss black paint applied with a thickness between 100 to 150 μm to provide a low reflectance coating such that the resulting BCU normal emittance is greater than 0.999. Temperature monitoring of the BCU is provided by two embedded 100-ohm platinum resistance thermometers (PRTs), with dynamic temperature control provided by a combination of liquid/gaseous nitrogen flow and servo control heaters contained in the rear of the BCU cone.

Two types of test sequences were used for the radiometric calibrations. In one sequence, the blackbody targets were stepped through a range of temperatures of interest while recording the thermal channel signal in response to target and PPR optical element temperatures. Similar tests were performed with the RCT-PPR replacing BCU-1. The second calibration sequence involved the sequential heating of individual optical elements (until

stabilized with a temperature rate of change less than 0.02 K min^{-1}), followed by cooling to the original temperature. The above sequences were used to determine the PPR thermal responsivity to changes in the scene- and space-view radiances, and to changes in optical element temperature, and thus establish the radiometric calibration coefficients for individual optical elements.

During the radiometric calibration tests, the instrument reference temperature was controlled to better than ±3 K. Typically, these tests were 8 to 10 hours in duration for the BCU temperature sequences and 12 to 16 hours for the optical element sequences. For both types of tests, significant variations in instrument temperature (and temperature gradients) were found to occur the course of testing at each 'nominal' instrument temperature. As a result, it was necessary to perform a least-squares solution to the set of radiometric equations representing optical element, scene-view, and space-view contributions to model the instrument response signal.

Figure 10 summarizes the results of an optical element heater test for a nominal instrument temperature of 5 °C. Here, the time scale (which is discontinuous) is expressed in terms of an index number of the individual tests performed. The solid line is a piece-wise continuous readout of instrument response in data numbers (DN) as individual heater elements are turned on and off, while the plotted points are the expected instrument response using the least-squares fitted calibration coefficients and the recorded optical element temperature variations. Tests of this type were conducted for each radiometry band over the expected instrument operating temperature range.

While these radiometric calibration tests provide a good understanding of the instrument response to the scene/space target signal and to changes in instrument temperature gradients, the thermal vacuum test simulations could not be expected to reproduce the precise thermal environment that will exist for the Galileo spacecraft in Jupiter orbit. Thus, inflight calibration testing will be used to verify and refine the calibration coefficients by sequentially viewing (with the scene-view telescope) the RCT-PPR and then space.

4.1.4. Polarimetric Calibration

Converting the measured signals for each polarimetry band to polarization degree and azimuth can be done in a number of ways using the three pairs of measurements obtained as the halfwave retarder is positioned with the retarder fast axis at 0°, 22.5°, and 45° with respect to the instrument reference direction. It is convenient to denote the measurement pairs (with the instrument off-set subtracted) at these three positions by M_{1S} and M_{1p}, M_{2S} and M_{2P}, and M_{3s} and M_{3p}, respectively, where '*S*' and '*P*' represent channel designations sensing the perpendicular and parallel polarization azimuths, respectively. At these positions, the action of the halfwave retarder produces an optical rotation of the linearly polarized components of the scene flux by - 2α, - 2α + 45 °, and - 2α + 90° where α is the azimuth of the linearly polarized component of the incident flux relative to the reference direction.

As indicated above, the third (45°) retarder position effectively produces an optical interchange of the roles of the S and P channels compared to measurements taken at the first (0°) retarder position. The optical interchange of channels provides a means to determine the responsivity ratio, *K*, relating the 'P' channel responsivity to the 'S' channel responsivity from

$$K = [(M_{1S}M_{3S})/(M_{1P}M_{3P})]^{1/2}.$$

Similarly, the effective hand passfilter ratio, C_2 (to account for any small difference of filter transmittance between the filters used for positions 1 and 2), can be determined from

$$C_2 = (M_{1S} + KM_{1P})/(M_{2s} + KM_{2P}),$$

with an analogous relationship for position 1 and position 3 measurements.

The components of the Stokes' vector of the scene radiance can then be expressed in terms of the above quantities as

$$I = M_{1S} + KM_{1P} = C_2(M_{2S} + KM_{2P}) = C_3(M_{3S} + KM_{3P}),$$

$$Q = KM_{1P} - M_{1S} = C_3(M_{3S} - KM_{3P}),$$

$$U = C_2(KM_{2P} - M_{2S}).$$

The polarization degree, P (in %), and azimuth, α, of the linear polarization of the scene follows as

$$P = (100/I)(Q^2 + U^2)^{1/2}, \quad \alpha = 0.5 \arctan(U/Q).$$

The photometry band measurements can also provide scene polarization information. These measurements are essentially equivalent to M_{1s} and M_{1p}. Thus, I and Q can be determined, and these are adequate to characterize the linear polarization of the scene in cases where the polarization azimuth is known (as can be established from measurements with the three polarimetry bands).

Polarization data reduction of cycle and PP/PH mode typically will use all six measurements obtained for each polarimetry band, i.e., outputs from both silicon photodiode detectors at each of the three successive retarder positions. While the desired radiance (when the appropriate instrument radiance responsivity factor is applied to I), linear polarization degree, and polarization azimuth constitute only three quantities to be determined, the redundancy of the six measurements can be exploited to monitor K, C_2, and C_3 or to improve the precision of the determination. In addition, since the intensity I is determined at each position, scene radiance changes are monitored throughout the measurements at the three retarder positions. Similarly, the equivalency of the position 1 and 3 measurements (see equation for Q) can be used to verify constancy of the scene polarization during the measurement period.

The approach of determining K, C_2, and C_3 from each set of the measurements has a disadvantage under special circumstances where K cannot be well-determined. Such a condition occurs when the radiance viewed has a linear polarization near 100% and the polarization azimuth is aligned nearly parallel or perpendicular to the PPR reference direction. In this situation, one term in the numerator and one in the denominator in the expression for K are near zero, and hence the equation is ill-conditioned. To avoid this problem, the data processing software was designed to allow the option to process the data using previously determined, read-in values of K, C_2, and C_3 The use of the appropriate read-in values has the additional advantage of better accuracy for calibration measurements since sufficient averaging of data can be used to eliminate any noise not associated with the quantization. (We note that K can be expected to be slightly dependent on the gain level being used since the gain step increments may be slightly different for the two channels.)

The calibration of the PPR polarimetry channels involved viewing various spatially uniform sources with predictable polarization characteristics. Scenes with linear polarizations approximating 100%, 8%, and 0% were used. Most of the measurements utilized either the standard lamp/reflectance standard or the optical calibrator unit (OCU). Since the xenon arc lamp in the OCU provides a near solar spectral distribution for the PPR 410 nm band, this yields a much better match to the expected spectral radiance of Jupiter, thereby improving the polarimetric accuracy for the intended application. For the narrow 678 nm band, either of the sources provides adequate source/scene spectral matching. The spectral line structure in the region of the 945 nm PPR band of the OCU xenon arc lamp together with the better stability of the tungsten filament lamp of the standard lamp/reflectance standard combination makes the latter source the preferred choice for the 945 nm band polarimetry calibrations.

To measure the instrumental polarization of the PPR, a low polarization source was viewed both with the PPR mounted in the usual orientation, i.e., with the instrument baseplate horizontal, and also with the PPR rotated about its optical axis by 90°. This was performed with the PPR mounted on the PPR handling fixture, since it is designed such that the PPR optical axis is equidistant from the two 'base' surfaces and also equidistant from the reference 'edge' for each of these surfaces. This allows the sources to be viewed sequentially with the PPR baseplate horizontal and then with the PPR baseplate vertical. Typical data taken to determine the PPR

instrumental polarization are given in Table V. Since the small polarizations measured change only slightly in magnitude and the azimuth also is little changed, i.e., follows the rotation of the instrument, it is apparent that the small polarization values measured for each band are primarily instrumental polarization. From the data it can be concluded that the PPR instrumental polarization is approximately 0.35%, 0.15%, and 0.40% for the 410, 678, and 945 nm bands, respectively. Correspondingly, it is found that the linear polarization of both the standard lamp/reflectance standard combination and the OCU is less than 0.1% for all three spectral bands, thus indicating that these source configurations have achieved the desired low degree of source polarization.

With either of the source configurations, the approach for both the high (near 100%) and moderate (near 8%) polarization conditions was to locate the polarizing element between the uniform radiance source and the PPR. For the near 100% linearly polarized radiance, two parallel dichoic polarizers mounted with the high transmission directions oriented parallel to each other were used. An HN22 polarizer set was used for the 410 and 678 nm bands with a similar HR polarizer set employed for the 945 nm band. When in use, a polarizer set was mounted on a rotatable stage which permitted the polarizer azimuth to be set accurately to any angle through a full 360° range. Similarly, a plane parallel plate of Schott WG280 glass was mounted such that it could be installed on the rotatable stage so that it remained tilted at 45° to the rotation axis of the stage during rotation. This rotatable tilted plate allows a known (caculable using the known wavelength-dependent refractive index of the plate via the Fresnel equations) linear polarization to be viewed, i.e., for the 410, 678, and 945 nm bands, P = - 8.32%, -8.06%, and -7.97%, respectively, at 45° angle of incidence. (These polarization values for the transmitted beam include the effect of multiple reflections and are averaged over an integral number of cycles of interference - justified due to the width of the spectral bands and the 2.5 mrad field of view of the instrument.)

4.2. INFLIGHT CALIBRATION

Several means of inflight calibration will be utilized by the PPR to update the preflight calibration of the photopolarimetry channels and to provide the prime radiometric calibration of the radiometry channel. These include: (1) an internal calibration lamp within the PPR aft optics; (2) the third orientation position for each of the halfwave retarders which interchanges the roles of the two silicon detectors; (3) the radiometric calibration target (RCT-PPR) that is separately mounted on the spacecraft and can function either as a blackbody source or to provide a slightly polarized lamp output signal for the visible/near-infrared region; (4) a spacecraft supplied photometric calibration target (PCT) that provides a standard of spectral radiance that can be viewed by all instruments located on the spacecraft scan platform; and (5) viewing stars and spatially unresolved planets.

4.2.1. *Internal Cal Lamp*

The small tungsten filament lamp located within the aft optics of the PPR provides a means to track any changes with time of the silicon detector/amplifier channels. The spectral output of the lamp is modified with the use of a color glass filter (Schott BG-18). The stability of this long-life (50 000-hour) lamp is further enhanced by operating it only intermittently, at a derated power level, and with a controlled, slow turn-on characteristic. The lamp is energized intermittently only during cycle mode operation while the chopper is being driven to its rest position following radiometry mode sampling at the solar + thermal filter wheel position and if the cal lamp command bit is set to the ON state. (The estimated total on time is less than 200 hours during the 7-year pre-launch testing period plus the post-launch inflight period.)

4.2.2. *Internal Polarimetric Calibration*

As previously discussed, one key feature for achieving accurate polarimetry with the PPR is the ability to cross-calibrate the detectors by measuring simultaneously the orthogonal polarization components of the scene radiance. The third halfwave retarder position (with fast axis oriented at 45° to the plane of deviation of the Wollaston prism) effectively interchanges the scene polarization components incident on the two detectors. This permits maintaining the polarimetric accuracy even in the presence of slow relative changes of the two detector channels with time. temperature, radiation, etc.

4.2.3. *RCT-PPR Design*

The RCT-PPR will serve in a dual calibration role for the PPR. The primary role will be as a thermal calibration target which closely approximates a blackbody source when viewed along the RCT-PPR axisymmetric axis. Due to spacecraft space limitations, it was necessary to restrict the overall length of the target. To achieve the desired

normal emittance ($\varepsilon > 0.998$) the geometry of the interior portion of the target has a truncated conical form with a center cylindrical section. This provides on-axis performance approximately equivalent to a cone with half the apex angle and twice the overall length. The end of the central cylindrical portion is not viewed by the PPR since this area is within the central obscuration of the PPR telescope. The interior of the target is a smooth (specularly reflecting) black-painted surface to achieve a higher on-axis emittance than would be possible with a rough (diffuse) surface for the same geometry. The calculated on-axis emittance of the RCT-PPR is greater than 0.998 based on the reflectance versus incident angle for the interior surfaces.

The RCT-PPR is designed and mounted such that it will be passively cooled at Jupiter to a temperature of 145 ±15 K. The wall thickness is chosen to assure worst case temperature gradients of less than 0.5 K. The temperature of the RCT-PPR is monitored by two platinum resistance thermometers (PRTs) that are calibrated by the manufacturer (resistance versus temperature) to an accuracy 0.2 K. These PRTs are read out directly by the PPR along with a low temperature coefficient resistor also mounted on the RCT-PPR to allow a first-order correction for spacecraft cabling resistance. The annular aperture of the target is designed to accommodate the 3-α worst case relative misalignments resulting from possible spacecraft environmental and mounting factors specified by the Galileo Project to assure that the PPR will view only the high emittance portion of the target during calibration. Through the use of the RCT-PPR and the preflight calibrations used to assess the influence of temperature changes of the PPR optical elements, it is expected that the overall radiometric calibration of the PPR thermal bands can be maintained within the desired ±1 K over the duration of the Galileo Mission.

A small tungsten-filament lamp is mounted in one portion of the RCT-PPR interior surface. With the source commanded ON, flux from the source passes through an elliptically shaped, plane-parallel sapphire plate mounted such that the outer surface approximately conforms to the inner conical surface of the target. The flux transmitted to the PPR is partially polarized due to different S and P Fresnel reflectances of the inclined plate. Thus, this source will be useful in assessing possible photometric and polarimetric changes of the entire optical train of the PPR over the course of the mission.

4.2.4. *Spacecraft PCT*

The PCT is intended to serve as a standard of spectral radiance for the scan platform mounted instruments by reflecting sunlight from a diffusely reflecting surface with well-characterized reflectance properties. Since this target can be viewed by all scan platform mounted instruments, the PCT is expected to be particularly useful in the role of calibration intercomparison among instruments.

4.2.5. *Viewing Astronomical Objects*

Orienting the PPR to view such astronomical objects as stars or spatially unresolved planets will be used to provide both cross-check of the absolute photometric calibration of the PPR silicon photodiode channels and as an additional means to track any responsivity changes with time, temperature, radiation, etc. Sirius is a star which will provide an adequate signal-to-noise ratio for this purpose by aggregating a sufficient number of samples. Similarly, viewing unresolved (object subtending less than the PPR field of view) planets at phase angles accessible from Earth will allow intercomparisons to be made with ground-based photometric calibration.

4.3. SIGNAL-TO-NOISE PERFORMANCE

4.3.1. *Photopolarimetry Channels*

Four separate band gains are used for the photopolarimetry channels, with the value applied (as described in the electronics section) being dependent on the filter/retarder wheel position as determined by the encoder. This will provide signal outputs of similar magnitude for the three polarimetry and seven photometry bands for typical scene spectral radiances. The channel and band gains were set to provide signal levels at Gain Step 8 of approximately 2000 DN for the three polarimetry bands (each with a separate band gain) and of approximately 1500 DN for the 648 nm photometry band (a single band gain is applied to all seven photometry bands). For setting these levels, the Jovian albedo values of Woodman *et al.* (1979) were used.

The noise of the photopolarimetry channels is essentially independent of signal level, resulting primarily from the 100 megohm feedback resistors in the pre-amplifiers. As a result, the signal-to-noise ratio (SNR) varies only slowly with temperature over the PPR operating temperature range (since the Johnson noise varies as the square

root of the absolute temperature). The measured SNR performance of the PPR photopolarimetry channels substantially exceeds the science-dictated, minimum SNR requirements of 1000 for the polarimetry bands and 200 for the photometry bands.

4.3. 2. *Radiometry Channel*

Achieving the SNR performance desired for the PPR science investigations utilizing the radiometry channel produces far greater stress on instrument design that is the case for the photopolarimetry channels. The inevitable Galileo mission mass and size constraints on science instruments required substantial compromise on performance characteristics. To optimize the SNR performance of the pyroelectric detector required thinning the $LiTaO_4$ detector element to the maximum extent possible. For the PPR application, ion-beam milling was used to provide thicknesses in the 5 to 6 μm range. In order to provide good optical absorption with low mass, the detector was coated with an evaporated gold-black coating. The wide range of absorbing characteristics found in the literature for gold blacks increased the risk with this approach, but on balance offered the best overall choice for the PPR requirements.

Optimization curves for the noise components of the PPR pyroelectric detector is illustrated in Figure 11. Measured noise data for the PPR detector were near the levels predicted. However, relative spectral response measurements indicated levels substantially below specification. The lower than expected long wavelength responsivity, combined with the lower than specified filter transmittance for some of the filters (much lower for the 37 μm band) led to the inability to meet the instrument SNR performance specifications for four of the seven radiometry channel bands. The measured versus specified SNR performance is indicated in Table VI. The solar plus thermal band measurement tabulated includes only the thermal component; the solar band is not included in the table, but comfortably exceeds the specifications. Three of the four out-of-spec bands have SNR performances about 60% of specification, while the 37 μm band (D filter) is about one-third of the desired level.

Fortunately the mission profile and the flexibility designed into instrument operation allows for observational 'work-arounds' to achieve nearly all of the anticipated science goals. The obvious approach of increasing the number of samples to improve the SNR (by the square root of the increase factor) is the principal observation strategy to achieve the radiometry science goals.

Acknowledgements

We wish to acknowledge the significant contributions made by many others in the development of the PPR experiment. In particular, we want to thank J. Hansen, who as Principal Investigator has provided direction and leadership for the PPR investigation, and former Co-Investigator D. Coffeen for his important contributions and insights. Other members of the PPR science team are M. Allison, A. Del Genio, and W. Rossow, all at the Goddard Institute for Space Studies; T. Martin and G. Orton at Jet Propulsion Laboratory; Y.-L. Yung at the California Institute of Technology, and P. Stone at the Massachusetts Institute of Technology.

Key supporting effort at SBRC in the design, development, and fabrication of the PPR instrumentation was provided by E. Aasted (electronic test), J. Abid (digital electronics), J. Bauer,Jr. (thermal analysis), S. Benda (quality assurance), J. Brooks (dynamic analysis), R. Cline (optical design), C. Coles (digital electronics and test), D. Errett (optical design), G. Hughes (system test), G. Hyde (software programming), W. Jefferies (optical procurement), W. Johnson (electronics packaging), H. Kleeburg (servo control), P. Olson (mechanical design), S. Pellicori (optical filters), F. Pineda (mechanical assembly), C. A. Rodil (reliability), H. Sanchez (electronic assembly), J. Shields (optical assembly), G. Stark (manufacturing process), and L. Watts (program management).

We express our thanks to our technical officers, M. Davis and A. Peterson of the Goddard Space Flight Center for their dedicated effort. Other key personnel providing essential support were the instrument coordinators, D. Griffith, G. McSmith, R. Parrish, and L. White; the science coordinators, N. Devine and T. Martin; and the science instrument manager, W. Fawcett, all with the Jet Propulsion Laboratory.

References

Hanel, R. A., Conrath, B. J., Herath, L. W., Kunde, V. G., and Pirraglia, J. A.: 1981, J. *Geophys. Res.* **86**, 8705.
Hunten, D. M., Colin, L., and Hansen, J. E.: 1986, *Space Sci. Rev.* **44**,191.
Pellicori, S. F., Russell, E. E., and Watts, L. A.: 1973, *Appl. Optics* **12**, 1246.
Seeley, S. J., Hunneman, R., and Whatley, A.: 1981, *Appl. Optics* **20**, 31.
Tomasko, M. G., West, R. A., and Castillo, N. D.: 1978, *Icarus* **33**, 558.
Watts, L. A., Russell, E. E., and Pellicori, S. F.: 1977, *SPIE* **112**, 28.
Watts, L. A., Russell, E. E., and Pellicori, S. F.: 1979, *SPIE* **172**, 326.
Weidner, V. and Hsia, J.: 1981, J. *Opt. Soc. Am.* **71**, 856.
Woodman, J. H., Cochran, W. D., and Slavsky, D. B.: 1979, *Icarus* **37**, 73.

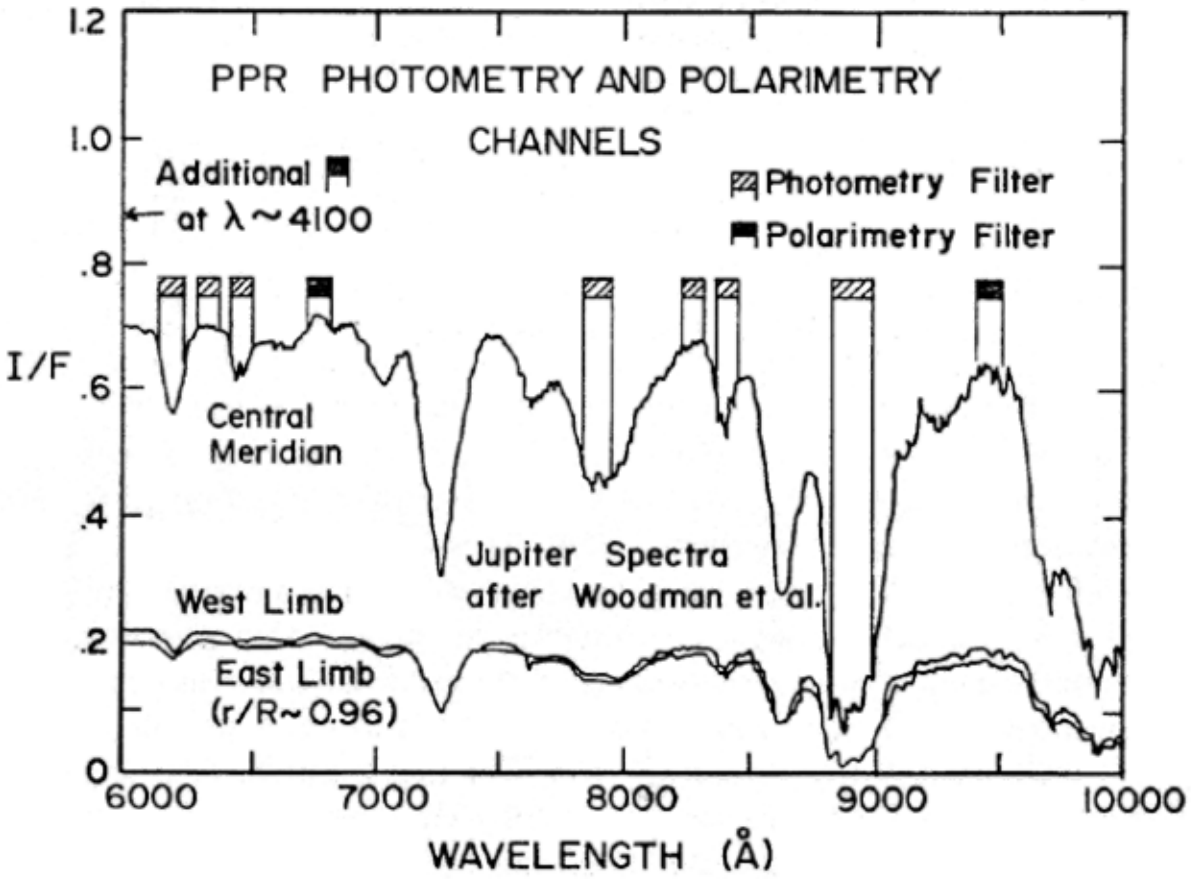

Fig. 1. Spectral locations of PPR photometry and polarimetry channels.

TABLE I
PPR filter spectral bandpasses

Mesurement function	Center wavelength	Full width at half max	Filter/retarder wheel position
Polarimetry	410.0 nm	60.0 nm	13, 15, 17
	678.5 nm	8.7 nm	7, 9, 11
	944.6 nm	10.8 nm	1, 3, 5
Photometry	618.7nm	7.0 nm	25
	633.3 nm	8.6 nm	26
	648.0 nm	7.4 nm	27
	788.7 nm	11.9 nm	28
	829.3 nm	11.9 nm	29
	840.3 nm	7.1 nm	30
	891.8 nm	11.1 nm	31
Radiometry	Solar + thermal	0.3-110+ μm	24
	Solar	0.3-4 μm	23
Channel: A	16.8 μm	4.2 μm	18
Channel: B	21.0 μm	3.0 μm	19
Channel: C	27.5 μm	7.2 μm	21
Channel: D	35.5 μm	6.9 μm	20
Channel: E	$\lambda > 45$ μm	45-110 μm	22

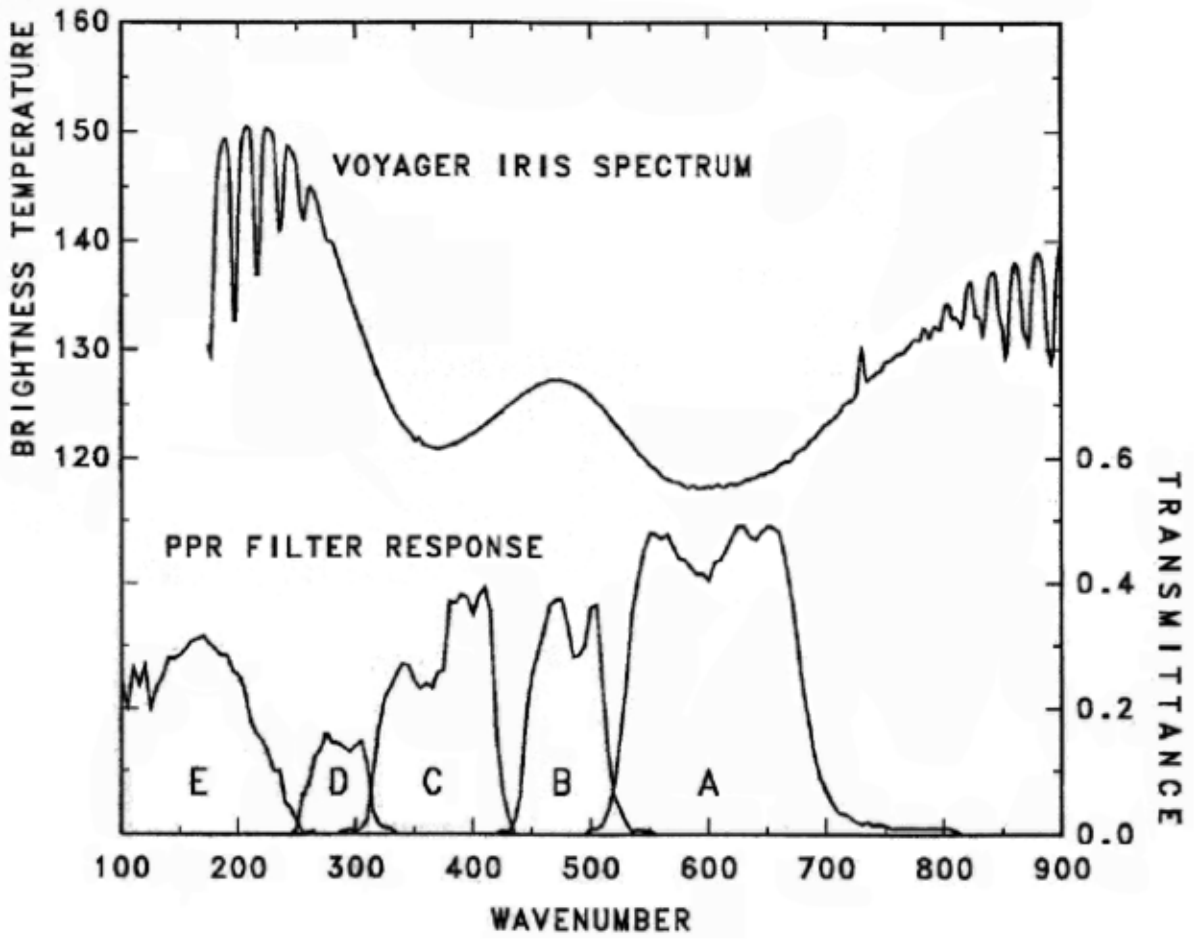

Fig. 2. Spectral locations of PPR thermal band relative to the Voyager IRIS spectrum of Jupiter.

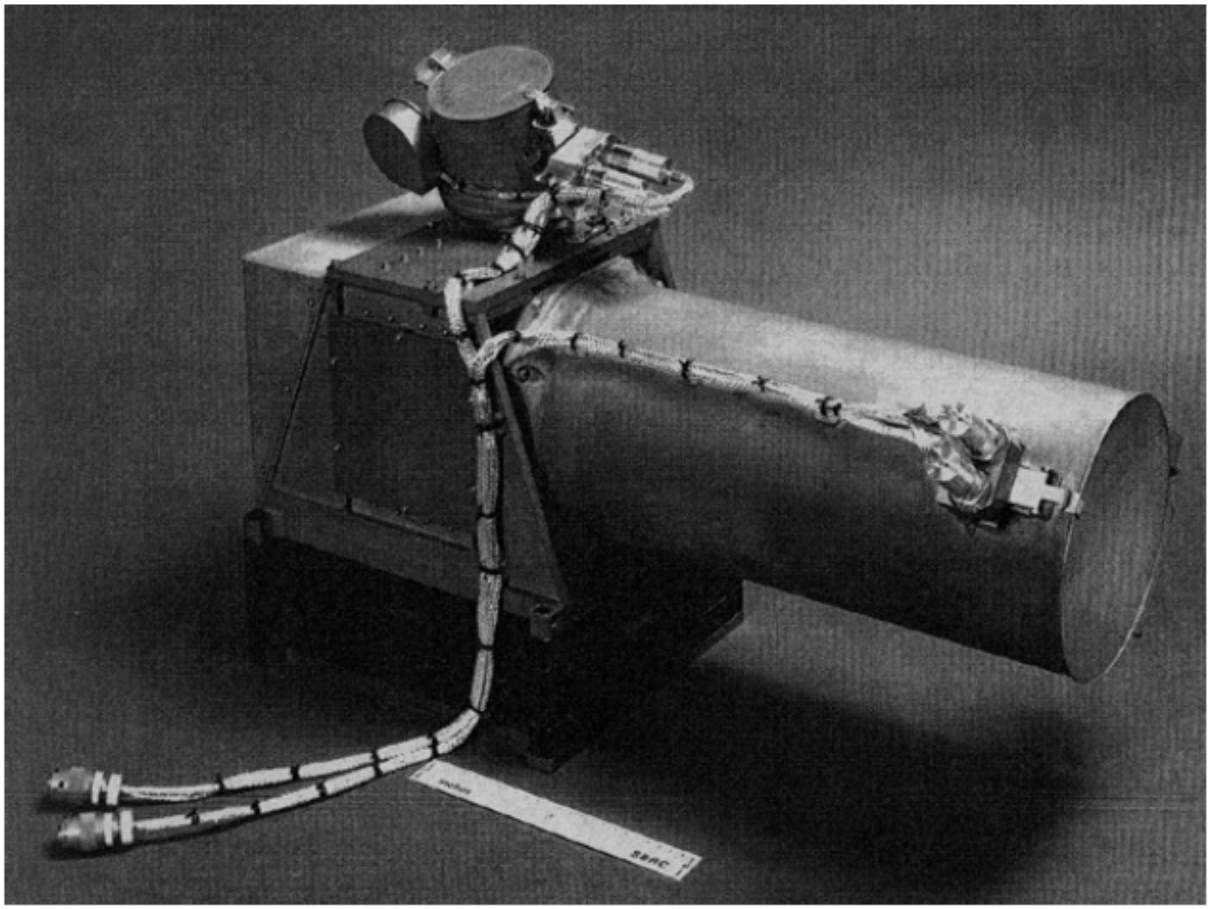

Fig. 3. The Galileo Photopolarimeter/Radiometer (PPR) with covers closed.

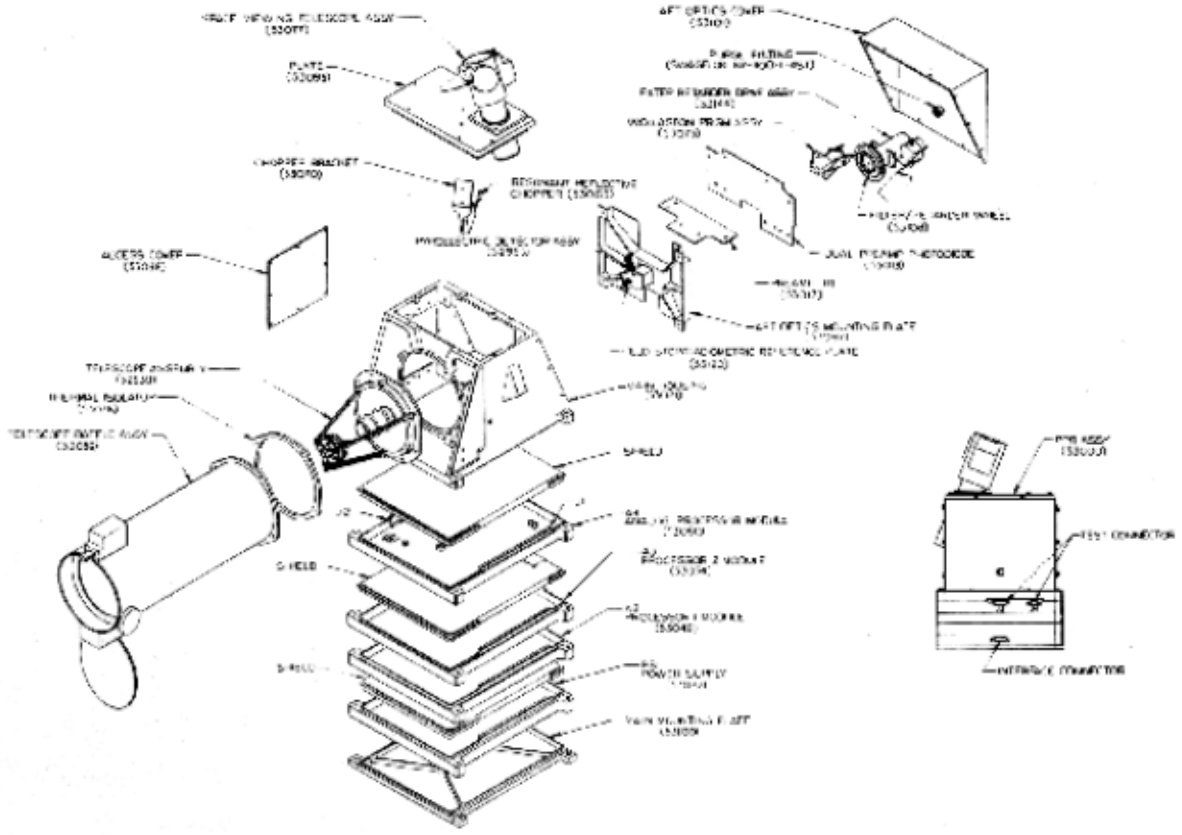

Fig. 4. Exploded view of the Galileo Photopolarimeter/radiometer (PPR).
Larger view (53 kB)

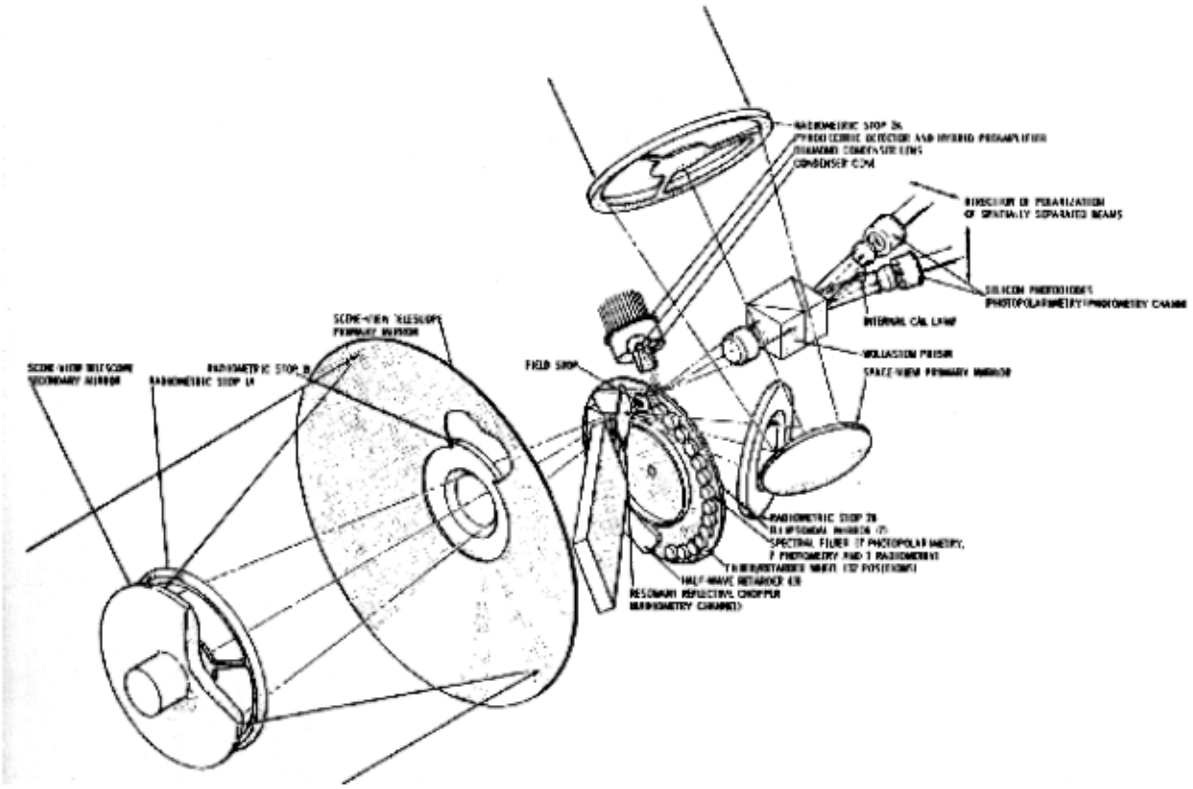

Fig. 5. Pictoral view of the Galileo Photopolarimeter/Radiometer (PPR) optical system.
Larger view (124 kB)

TABLE II
Photopolarimeter/radiometer instrument parameter summary

Telescopes	Cassegrainian type (10-cm aperture diameter, 50--cm effective focal length) for scene view and plane mirror system for space view
Command	One configuration control command (three 8-bit bytes)
Interface signals	interface bus signals (CDS RTI, CDS supervisory data and reply data); 30 VDC; replacement heater; radiometirc calibration target temperature sensors and external cal lamp; and bellows actuator power
Data format	48 bits status plus 96 bits science sample related data
Data rate	144 bits (buffer fill) every minor frame (2/3 s) or 216 bps
Location	Instrument located on scan platform
Viewing and pointing requirments	Instrument optical axis aligned parallel to that of the SSI, and radiometric calibration target for PPR to be viewable occasionally; direct viewing of the Sun to be avoided except on a transient basis
Temperature limits	+50 °C to -40 °C design range; +40 °Cto -30 °C protoflight test range

Size	44.8 x 39.1 x 32.7 cm
Mass	5.2 kg (11.4 lb.) including radiation shielding
Power	11.0 W (peak); 3.8 W (filter/retarder motor, chopper and cal lamp off); replacment heater (actuates contamination covers) 4.5 W

	Photopolarimentry	Photometry	Radiometry
Spectral bands	410 nm ($\Delta\lambda = 60$ nm) 678 nm ($\Delta\lambda = 9$ nm) 945 nm ($\Delta\lambda = 10$ nm)	618 nm ($\Delta\lambda = 9$ nm) 633 nm ($\Delta\lambda = 10$ nm) 646 nm ($\Delta\lambda = 8$ nm) 789 nm ($\Delta\lambda = 12$ nm) 830 nm ($\Delta\lambda = 10$ nm) 841 nm ($\Delta\lambda = 7$ nm) 892 nm ($\Delta\lambda = 12$ nm)	Solar ($\lambda < 4$ µm) Solar plus thermal (no filter) 17 µm($\Delta\lambda = 4$ µm) 21 µm ($\Delta\lambda = 4$ µm) 27.5 µm ($\Delta\lambda = 9$ µm) 37 µm ($\Delta\lambda = 10$ µm) $\lambda > 42$ µm
Instantaneous geometric field of view	2.5 mrad circular	2.5 mrad circular	2.5 mrad circular
Detectors	Two enhanced silicon photodiodes (1.5-mm diameter) operated in photovoltaic (unbiased) mode	Same as detectors used for photopolarimetry	One lithium tantalate pyroelectric detector (0.57 mm circular)
Inflight radiometric calibration	Internal and external inflight calibrator lamps: science photometric calibration target	Internal and external inflight calibrator lamps: science photometirc calibration target	External inflight calibartion lamp; PPR radiometric calibration
Polarization analyer and calibration	Symetrical Wollaston prism analyer; achromatic half-wave retarders (optimized for each spectral band) positionable to produce x + 0°, x + 45°, and x + 90°, rotations	Symmetrical Wollaston prism analyzer	Not applicable
Analog/digital conversion	12-bit A/D conversion of the two analog signal channels	12-bit A/D conversion of the analog signal channels (7- to 80bit precision required with remainder of range utilized to assure adequate gain balance margin)	12-bit A/D conversion of the analog signal channel (7- to 8-bit precision required with remainder of range utilized to assure adequate gain balance margin)

integration and sampling	Two channels simultaneously sampled (217 ms integraion period) for 1, 4, 16, 256 samples per position	Two channels simultaneously sampled (217 ms integration period) for 1, 4, 16, or 256 samples per position	One channel sampled (433 ms integration period) for 1, 4, 16, or 256 samples per position
Measurement accuracy	Polarimetric: ± 0.1% Absolute radiometric: ±3% (precision better than 1%)	Absolute radiometric: ± 3%	Absolute radiometric for solar reflectance band: ± 5% Absolute radiometric for thermal emmission: ± 1 K (at 130 K)

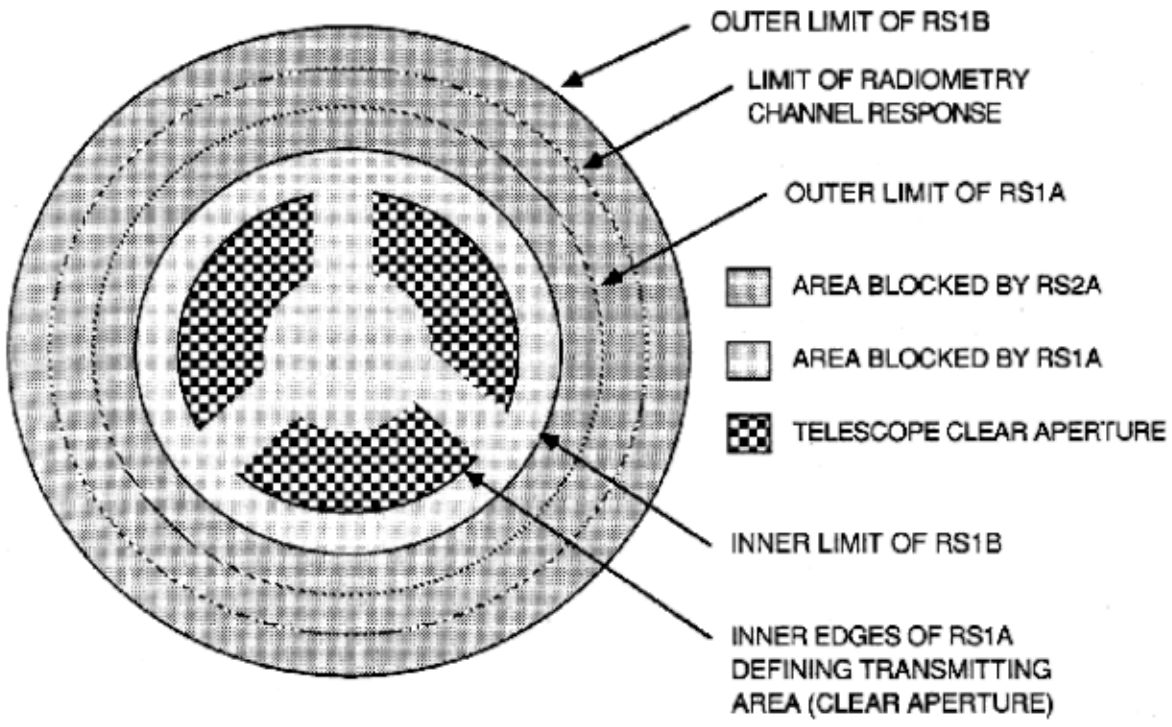

Fig. 6. Field-of-view angular blocking by radiometric stops.

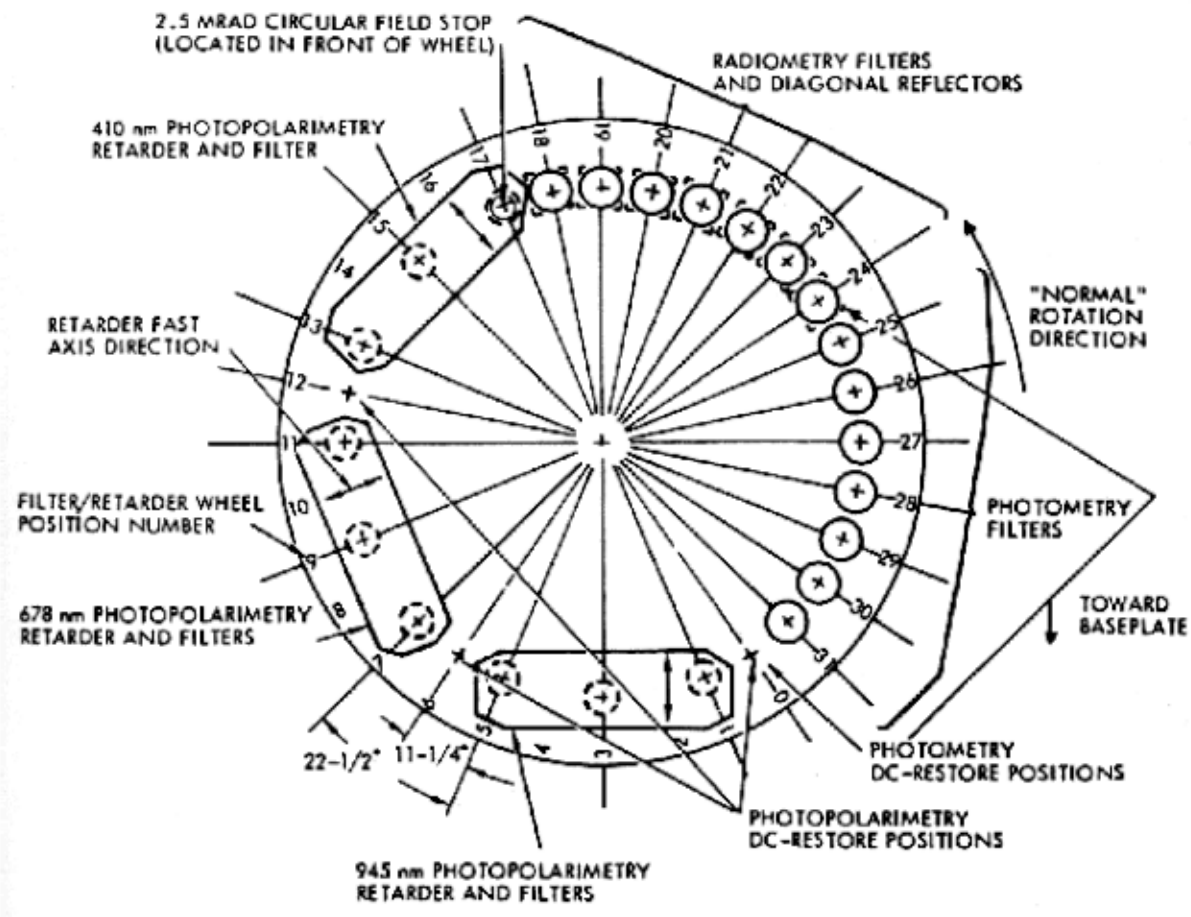

Fig. 7. Galileo PPR filter/retarder wheel layout (looking into telescope apeture).

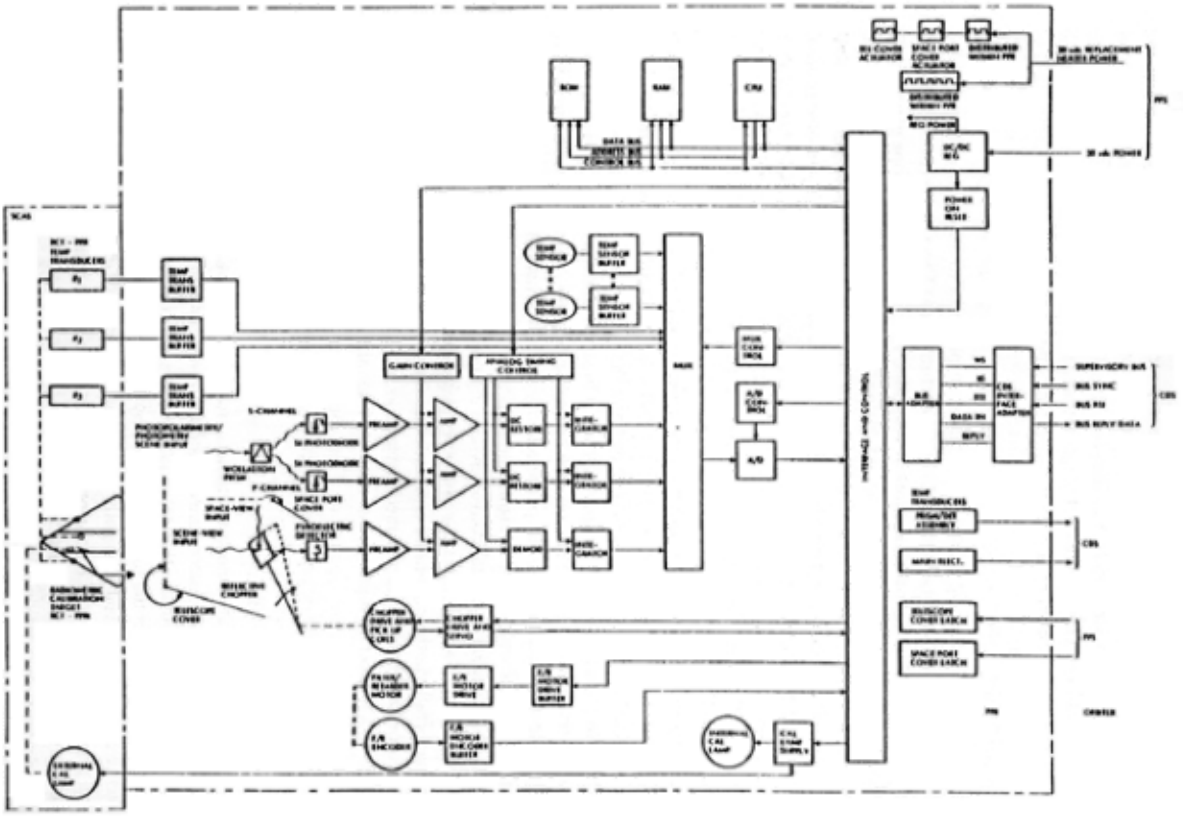

Fig. 8. Galileo PPR and RCT-PPR functional blocking diagram.
Larger View (235 kB)

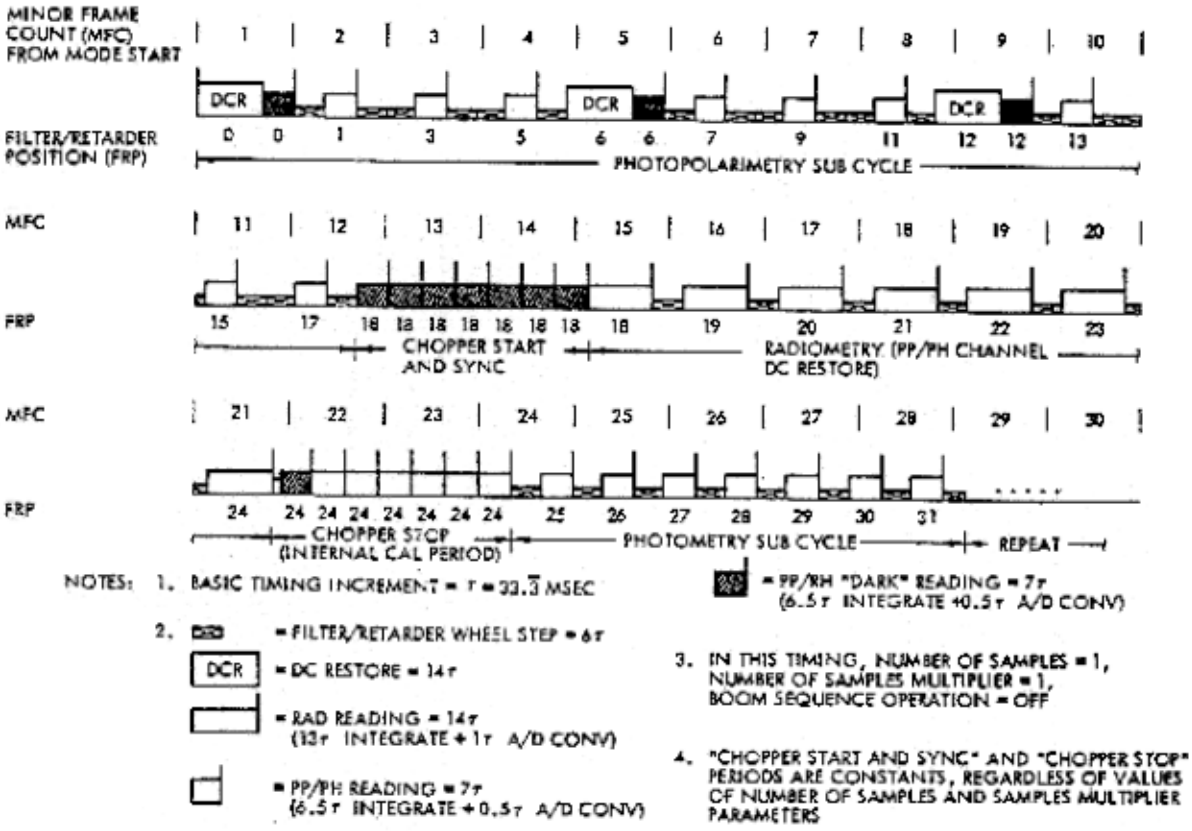

Fig. 9. Galileo PPR cycle mode sample timing diagram. Cycle shown requires 18.8 s (28.2 minor frames) for the parameter vlaues indicated.
Larger View (60 kB)

TABLE III
Commandable function of Galileo photopolarimeter/radiometer (PPR)

Command	Command function
Power on	1. PPR is set to 'cycle mode at power 'on' with gain step PP/PH=5, gain set rad=0, number of samples=256, number of samples multiplier=0, cal lamp=1, dc-restore initiate=1, boom sequence operation=0, temperature range select=0, and chopper heater=0
Mode	1. Selects PPR mode from among cycle, photopolarimetry plus photometry (PP/PH), photometry (PH), radiometry (RAD), and position select modes 2. Initiates operations of selected mode after reaching starting filter/retarder position wherein: A. Filter/retarder wheel is stepped, and

B. sampling and dc-restoration occur as appropriate for selected mode

Programmed filter/retarder position	1. Selects filter/retarder position to be used as starting position when position select mode in operation
Gain step PP/PH	1. Selects gain setting for photopolarimetry/photometry channels from among 16 levels with each being separated from adjacent levels by a factor of approximately 1.4
Gain step rad	1. Selects gain setting for radiometry channel from among four levels
Number of positions	1. Selects number of positions in addition to programmed filter/retarder postion (starting position) from among 0,1,2 and 5 when position select mode is operating
Number of samples	1. selects number of samples of data to be accumulated at each active filter/retarder wheel position from among 1, 4, 16, and 256 2. In position select mode, the commanded number of samples shall be unused as the number of cycles of position selected operation occurring prior to dc-restoration
Number of samples multiplier	1. Selects multipler for number of samples as either 1 or 4, depending on whether bit is a 0 or 1, respectively 2. Increases the number of samples by the selected factor for the radiometry channel sampling only (256 maximum) 3. If external cal lamp is activated (see below) selects on period to be either six samples or the total number of smaples to be taken during roll when bit is 0 or 1, respectively
Cal Lamp	1. enables or inhibits pre-programmed calibrator lamp operation depending on whether command bit is 1 or 0, respectively 2. Enables external cal lamp, if bit is a 1 and if boom sequence operation bit is also a 1 (with duration controlled as noted above.) If either of these control bits is 0, the external cal lamp operation is inhibited
DC-restore initiate	1. Initiates special dc-restore cycle in position select mode or boom sequence operation wherein: A. Filter/parameter wheel is stepped to appropriate dc-restore position B. dc-restoration function in performed followed by a single dark sample, and C. Filter/retarder wheel is returned to next fitler/retarder position of the sequence of the selected mode
Boom sequence operation	1. Normal stepping of filter/retarder wheel is inhibited (except in transition mode) 2. Stepping between adjacent functional filter/retarder positions is initiated once per roll based upon receipt of spacecraft spin angle

	and spin rate data 3. Affects external cal lamp operation as noted above under cal lamp
Temperature range select	1. Selects initial high or low range for thermistor temperature sensors depending on whether bit is a 1 or 0, respectively. Where thermistor output is out of range, software switches range as appropriate
Chopper heater	1. Initiates heating of chopper mirror when bit is 1 with function disabled when bit is 0

TABLE IV
Selected preflight calibration tests for the Galileo PPR

Test name	Measurement procedure
Radiometry (RAD channels except solor band)	View BCUs at various temperatures in T/V chamber while varying PPR optical element heaters with BCUs held at < 188 K
Radiometirc calibration (POL/PH channels plus solar and S + T channels)	View halon reflectance standard illuminated by standard lamp (irradiance standard)
Gain/linearity (POL/PH channels plus S+T bands)	Measure PPR gain steps by viewing OCU with various selected OCU neutral density filters
Signal-to-noise performance	Collect applicable data during radiometric calibrations and gain and linearity testing
Polarimetric calibration	View OCU and/or standard lamp/reflectance standard with and without interposing rotatable polarizing elements for the PPR in its normal orientation and rotated by 90°
Relative spectral response	Measure spectrophotometer output with PPR 410 nm, solar and S + T bands with a calibrated silicon photodiode or electrically calibrated pyroelectric detector. Cascaded optical element measurements used for other bands
Temperature-dependant response	Performed as part of T/V calibration testing with BCUs or the OCU viewed with the PPR at various temperatures
Air-to-vacuum responsivity shift	Measured by viewing OCU through T/V chamber window with chamber at ambient pressure and evacuated

Integrated spectral out-of-band response	View knows sources through colored glass and other materials with well defined cut-on/cut-off characteristics
Field-of-view response	view source of small angular subtense scanned across PPR field of view
Scattered light (off-axis) response	View extended solar illuminated white target with a central Circular portion of target removed and with target intact. Direct off-axis viewing of Sun for > 18° off-axis response
Optical axis alignment	Compare alignment of field stop center and alignment mirror to PPR reference surfaces using theodolite

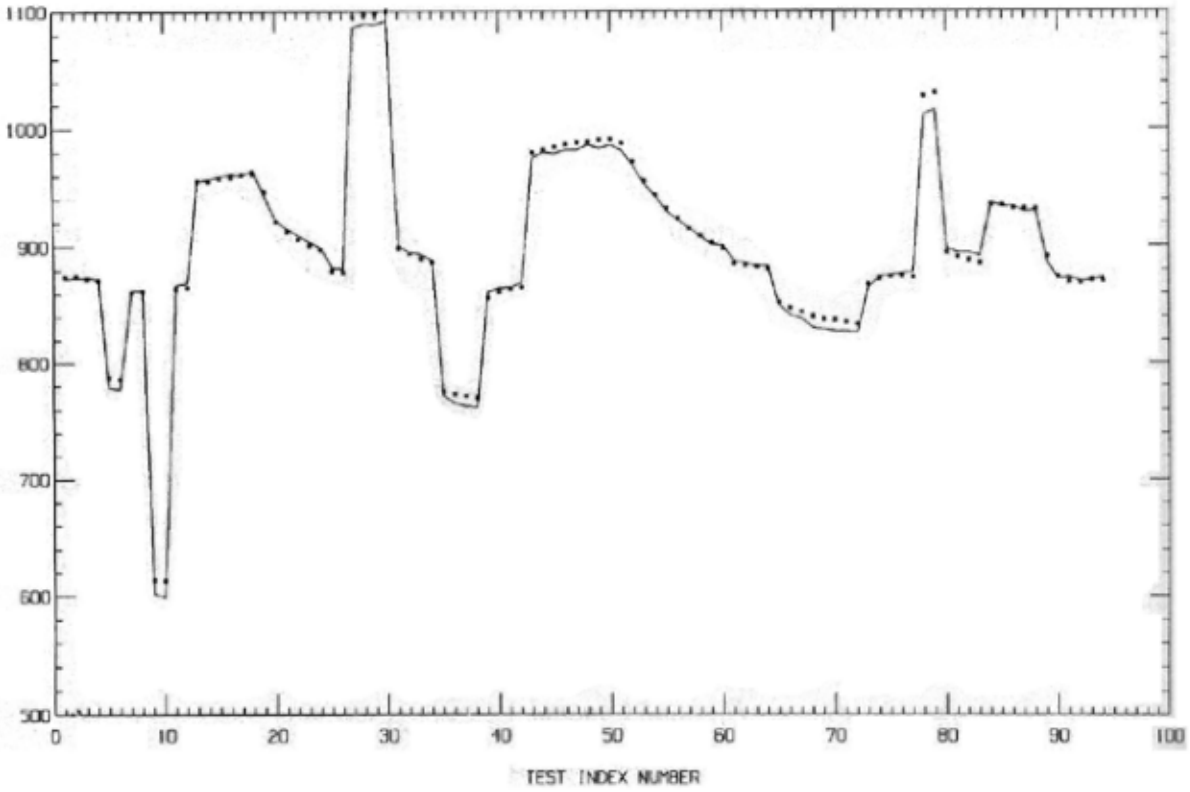

Fig. 10. Sample thermal/vacuum optical element heater test summary at + 5 °C.

TABLE V
Typical data to determine instrumental polarizaion
Measured degree of polarization in %, (azimuth in deg)

Source used	PPR in normal orientaion	PPR rotated 90°:

	945 nm	678 nm	410 nm	945 nm	678 nm	410 cm
Optical calibrator unit	0.38	0.10	0.29	0.42	0.15	0.40
	(18.0)	(143.8)	(165.8)	(15.4)	(155.7)	(167.6)
Standard lamp and reflective standard	0.46	0.13	0.34	0.35	0.18	0.36
	(18.6)	(159.7)	(170.2)	(12.2)	(142.9)	(164.7)

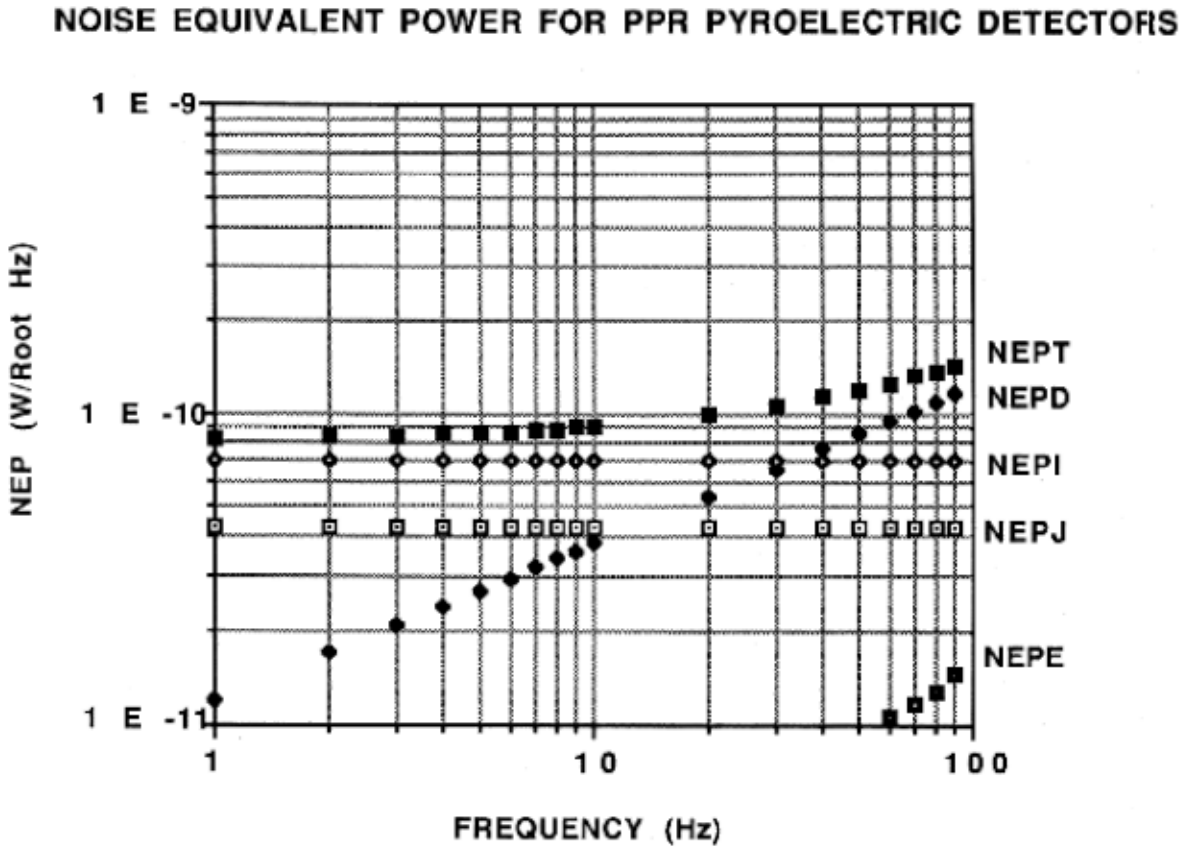

Fig. 11. Galileo PPR pyroelectric detector channel noise equivalent power (NEP). NEPT is a total root-sum-squared combination of the NEP components due to: dielectric loss tangent noise (NEPD); pre-amplifier FET gate leakage current noise (NEPI); pre-amplifier volatge noise (NEPE); and Johnson noise of the detector load resistor (NEPJ).

TABLE VI
Measured vs Specified signal-to-noise performance for PPR radiometry

Radiometry Band	Signal-to-noise ration (SNR)[a]	
	Measured[b]	Specification
17.0 μm	30	30
21.0 μm	20	35
27.5 μm	41	65
37.0 μm	12	40
$\lambda > 42 \pm 3$ μm	33	50
Solar + Thermal	460[c]	250

[a] SNR values are based on 4-sample averages with an instrument temperature of 0 °C.

[b] Data corrected to correspond to a 130 K blackbody scene (data measured with BCU-1 = 180 K and BCU-2 = 88 K.)

[c] Measurment on ly inclueds thermal component for a 130 K balckbody scene